Available online at www.sciencedirect.com
ScienceDirect
Journal of the European Ceramic Society 31 (2011) 1703–1712
www.elsevier.com/locate/jeurceramsoc

Mechanical and elastic properties of fine-grained polycrystalline scandia and erbia as determined by indentation techniques

Ori Yeheskel [a,b,*], Ismail C. Albayrak [a], Babak Anasori [a], Michel W. Barsoum [a]

[a] Department of Materials Science and Engineering, Drexel University, Philadelphia, PA 19104, United States
[b] NRCN, Be'er Sheva 84190, Israel

Received 2 December 2010; received in revised form 28 February 2011; accepted 16 March 2011
Available online 14 April 2011

Abstract

The Young's moduli, E, and nanoindentation, NI, stress–strain curves of fine-grained scandia, Sc_2O_3, and erbia, Er_2O_3, were determined using spherical indenters with radii of 1.4 μm and 5 μm. The Young's moduli measured with the spherical indenters, were comparable to those measured by a Berkovich tip, and by ultrasound. This work further validates the use of S vs. a plots to measure the Young's moduli of polycrystalline ceramics. A major advantage of using this technique is the possibility of determining NI stress–strain curves and concomitant yield points, apparent strain hardening rates, etc. for the first time. Both the elastic moduli and the yield stresses were affected by the degree of surface polishing and tip size. The most reproducible and reliable results were obtained with the sharper nanoindenter and the best surface finish. The Vickers hardness and indentation fracture toughness values extracted from the Vickers indentations are comparable to the literature results.

Keywords: Mechanical properties; Elastic modulus; Nano-indentation; Er_2O_3; Sc_2O_3

1. Introduction

Scandia, Sc_2O_3 and erbia, Er_2O_3, are cubic sesquioxides. Scandia that resembles light element binary rare earth sesquioxides (R_2O_3)[1] – is sometimes considered for high temperature applications[2–4] and is also considered as a host material for solid-state lasers,[5–7] and as a heat-resistant optical window in solid-state laser.[7] Erbia, Er_2O_3 possesses high thermal stability and corrosion resistance and is used accordingly.[8,9]

Data on the elastic moduli and strengths of Sc_2O_3 are scarce,[2,3,10–13] and so are the elastic and mechanical properties of Er_2O_3.[8,9,13,14] Table 1 summarizes the literature data on the elastic moduli of Sc_2O_3 and Er_2O_3 over the last 40 years. Gazza et al. report a Young's modulus in bending for transparent scandia.[2] Gogotsi claimed that the elastic modulus of Sc_2O_3, determined from 4-point flexure experiments, depended on sample size.[3,12] Dole et al. report the dynamic elastic moduli of porous Sc_2O_3 and estimated an extrapolated value for a pore free material.[11]

In addition to direct measurements the Young's moduli, E, can be also calculated knowing the bulk moduli, B, and Poisson's ratios, ν. Bulk moduli, B, can be either measured or estimated. Estimation of the bulk moduli of R_2O_3 compounds using various techniques/assumptions are listed given in Table 1.[15] The bulk modulus can be measured isothermally e.g. using a diamond anvil cell[16,17] or using dynamic methods.[11,17] Based on the compiled B values in Table 1, and the Poisson's ratio, ν, of fully dense Sc_2O_3, viz. 0.257,[11] the calculated E values are in the range of 261 ± 35 GPa. This ∼14% scatter is too high for any material.

For Er_2O_3, the E of slightly porous samples, and extrapolated to full density, was reported to be ∼175 GPa.[18] Recently, the elastic constants of Er_2O_3 single crystals were measured from which an $E \sim 177$ GPa was calculated for polycrystalline samples.[14]

The Berkovich or Knoop hardness values of Sc_2O_3 were measured by a number of researchers and summarized in Table 2.[2,19] The hardness and indentation fracture toughness of single crystal and sintered Er_2O_3 are also summarized in Table 2.[8,9,20,21] For erbia it was reported that the hardness decrease and the fracture

* Corresponding author at: NRCN, Be'er Sheva 84190, Israel. Tel.: +972 86567365; fax: +972 86569111.
E-mail addresses: oriyehe@gmail.com, yeheskel_ori@hotmail.com (O. Yeheskel).

0955-2219/$ – see front matter © 2011 Elsevier Ltd. All rights reserved.
doi:10.1016/j.jeurceramsoc.2011.03.030

Table 1
Summary of the elastic properties of high density Sc_2O_3 and Er_2O_3; density, ρ, and dynamic Young's moduli E, shear moduli, G, adiabatic bulk moduli, K_S, isothermal bulk moduli, K_T, and Poisson's ratio, ν from various sources. For Sc_2O_3 the Young's moduli values in parentheses were calculated from the isothermal bulk moduli assuming $E = 3K_T(1-2\nu)$, and a Poisson's ratio of 0.257 of Dole et al.[11]

Source	ρ (g/cm^3)	E	G	K_S or K_T	ν	Ref.
Sc_2O_3						
Gazza et al. 1971		241				[2]
Gogotsi 1980	3.79	218				[3]
Gogotsi 1980	3.79	251				[3]
Dole et al. 1977	3.795	214.3	86.7	135.2	0.236	[11]
Dole et al. 1977[a]	3.818	221.4	89.0	144.0	0.244	[11]
Dole et al. 1977[b]	3.841	227.6	90.5	156.2	0.257	[11]
Makino et al.; 2000	(3.841)	(184–244)		126-167	(0.257)	[15]
Yusa et al.; measured 2009	(3.841)	(275 ± 10)		189 ± 7	(0.257)	[16]
Yusa et al.; calculated 2009	(3.841)	(290)		199	(0.257)	[16]
Barzilai et al.; measured 2010	(3.841)	(284 ± 6)		195 ± 5	(0.257)	[17]
Er_2O_3						
Manning et al.; 1969[a]	8.20	155.7	60.2	125.9	0.294	[18]
Manning et al.; 1969[a,b]	(8.66)	175.2	67.8	140.7	0.292	[18]
Sharif et al.; 2000	(8.66)	177.36	66.23	183.6	0.339	[14]

[a] Data taken from the National Institute of Standards and Technology (NIST) database.[13]
[b] Extrapolated values to zero-porosity.

toughness increase with the increase of temperature from room temperature to 1200 °C, and above.[8,9,20] The room temperature single notch edge beam K_{IC} of Sc_2O_3 was measured by Gogotsi et al. to be ≈1.5 MPa m$^{1/2}$.[3,12,22]

The idea to use indentation methods for evaluating stress–strain curves in metals was put forward six decades ago.[23] More recently, micro-indentation[24] and nanoindentation, NI,[25–30] techniques have been put forth to study the elastic moduli and hardness values of metals and other materials. Today NI – mostly with sharp Berkovich indenters – is a common technique used to measure the hardness and moduli values of a large range of materials and thin films.[24–31]

Recently, a technique was developed to generate NI stress–strain curves from spherical NI load/displacement curves. To date this technique has been applied mainly to ceramic single crystals.[32–38] Recently, we applied this method to study the elastic and mechanical properties of fine-grained polycrystalline yttria,[39] and showed that the E values – calculated from the stiffness, S, vs. a curves (see below) – where a is the contact radius – were ≈5% lower than the 176 GPa value measured by ultrasound on the same sample. Based on that work, we concluded that S vs. a plots are a powerful, and relatively simple, technique to measure the E of polycrystalline ceramics, and other hard solids. The fact that one also obtains NI stress–strain curves is a distinct advantage over the more commonly used Berkovich tip.

The objective of this paper is to characterize the room-temperature mechanical and elastic properties of 98.5+% dense, fine-grained Sc_2O_3 and Er_2O_3 using the aforementioned technique. We also generate NI room temperatures stress–strain curves for Sc_2O_3 and Er_2O_3, with grain sizes of ≈1 μm and 3 μm, respectively, for the first time. The Vickers hardness and Vickers indentation fracture toughness were also measured for both materials.

2. Theoretical considerations

2.1. Spherical NI

Load (P) and total displacement into the surface (h_t) values were collected by the NI. The harmonic contact stiffness

Table 2
Summary of the relative density, ρ^*, hardness values in: Knoop, H_K, Berkovich, H_{Br}, and Vickers, H_V, and the fracture toughness, K_{IC}, of Sc_2O_3 and Er_2O_3 from various sources and processing routes.

Source	ρ^* [%]	H_K [GPa]	H_{Br} [GPa]	H_V [GPa]	K_{IC} [MPa m$^{1/2}$]	Ref.
Sc_2O_3						
Gazza et al. 1971, HP*, transparent	~100	8.9				[2]
Gogotsi 1980 sintered	98.7				1.49	[3,12,22]
Xu et al. 2001 thin film 450 °C	~100		8.3			[19]
Xu et al. 2001 thin film 600 °C	~100		11.4			[19]
Er_2O_3						
Petrovic et al. 1997 SC+	~100			7	2.50	[8]
Petrovic et al. 1998 SC	~100			9	0.86	[9]
Sharif et al. 2000 SC	~100			7	0.8	[14]
Neuman et al. 1997 SC	~100			6	1.8	[21]
Neuman et al. 1997 Sintered	~90			6	~3.0	[20]

HP*, hot pressed; SC+, single crystal.

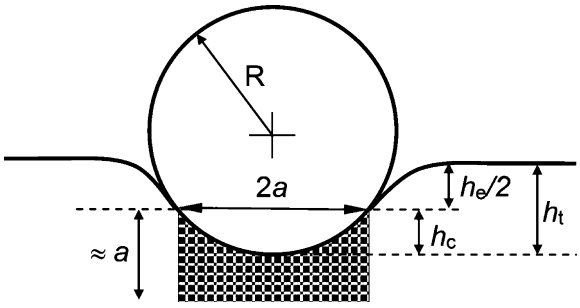

Fig. 1. Schematic of spherical indenter and associated terms used in text.

(S) values were measured continually – by superimposing a small harmonic signal to the increasing load applied during the nanoindentation.[25,30] The basis of the method is described elsewhere.[27–32] Briefly, the contact radius (a), is related to the spherical tip radius (R), and on the contact depth (h_c) (Fig. 1). The latter is calculated assuming[30,32]:

$$h_c = h_t - \frac{3}{4}\frac{P}{S} \tag{1}$$

The contact radius, a, is then calculated assuming[30,32]:

$$a = \sqrt{2Rh_c - h_c^2} \tag{2}$$

The stress is related to the strain using assuming[31,32]:

$$\frac{P}{\pi a^2} = \frac{4}{3\pi}E^*\left(\frac{a}{R}\right) \tag{3}$$

The left side of the equation is the indentation stress, sometimes referred to as the Meyer hardness, and a/R is the indentation strain. E^* is a reduced modulus given by:

$$\frac{1}{E^*} = \frac{1-\upsilon^2}{E} + \frac{1-0.07^2}{1140} \tag{4}$$

where ν and E are the Poisson's ratio and Young's moduli of the sample, respectively. The other numbers are the corresponding values for the diamond indenter tip. The Poisson's ratios for Sc_2O_3 and Er_2O_3 were, respectively, assumed to be 0.288 and for 0.299 (see below).

Given that for an isotropic elastic solid, indented with a spherical indenter,[15–17]

$$S = 2aE^* \tag{5}$$

it follows that the slope of S vs. a plots should yield E^*, from which the spherical NI Young's modulus, E_{Sp}, is calculated from Eq. (4). In general one of the problems in interpreting NI results is determining the first point where the indent hits the surface, viz. the zero point.[26] Over the years various methods have been proposed to perform this zero-point correction.[26,31] We used a recent method devised by Moseson et al.[33] The main advantage of this method, in addition to its simplicity, is that it essentially – by forcing the S vs. a curves through the origin – ignores the initial data points.[33,39]

3. Experimental

3.1. Sample processing

A 99.95% pure Sc_2O_3 powder (China Rare Metals Material Co. Ltd, China) with an average particle size of <1 μm, was cold isostatically pressed at 300 MPa. The compacts were heat-treated in air, using a proprietary treatment, followed by a 24 h vacuum (~3 Pa) treatment at 800 °C to dry them. The pressed and treated compact was then hot isostatically pressed (HIPed) at 1300 °C under a pressure of 130 MPa for 5 h.[4]

For Er_2O_3, a 99.9% pure powder (China Rare Metals Material Co. Ltd, China) was compacted and processed using a procedure identical to that used for the fabrication of transparent yttria described elsewhere.[40] Briefly the cold pressed pellets were dried and then HIPed at 1350 °C under a pressure of 150 MPa for 1.5 h.

A ≈8 mm thick slice of Sc_2O_3 was used in the present study. The sample surfaces were ground parallel to each – to within ±1 μm of parallelism, other using 600 grit polishing paper – for the determination of its dynamic elastic modulus. The beige HIP'ed Sc_2O_3 sample was mounted (Fig. 2a, inset) and polished with 1 μm diamond paste before testing. The cross section revealed four areas, with different tones of beige. These areas – all defined in the inset in Fig. 2a – are hereafter designated as: Center, Ring, Outside and Rim.

The opposite sides of a 2.7 mm thick pink, HIPed Er_2O_3 sample, were also ground parallel to each other using a 600 grit polishing paper prior to the determination of its dynamic elastic modulus. The sample was then glued to a sample holder and polished down to 1 μm for the NI and other hardness measurements (Fig. 2c, inset).

During preliminary work, we realized that surface finish affected the measured NI yield points and moduli, with finer surfaces yielding more accurate results. Consequently, all results reported herein were obtained on surfaces that were polished down to 0.25 μm diamond suspension. The effects of surface roughness on properties are discussed in detail in a separate paper.

3.2. Material characterization

3.2.1. Dynamic elastic moduli

The dynamic elastic moduli, E^S, were calculated from the longitudinal and transverse sound velocities, V_L and V_T, respectively, measured on the same samples used for the indentation tests. The velocities were measured using a pulse-echo method described elsewhere.[40] The sample's density, ρ, was measured using Archimedes' method.[41] The uncertainty in the density measurements is estimated to be ≈±0.1%; that in $V_L \approx \pm 0.1\%$, and that in $V_T \approx \pm 0.1\%$. The resulting uncertainty in E^S is thus better than 1%, while that of the dynamic Poisson's ratio, ν^S, is about 3%.

3.2.2. Spherical nanoindentation

A nanoindenter (XP System, MTS, Oak Ridge, TN) with a continuous stiffness measurement (CSM) attachment was used.

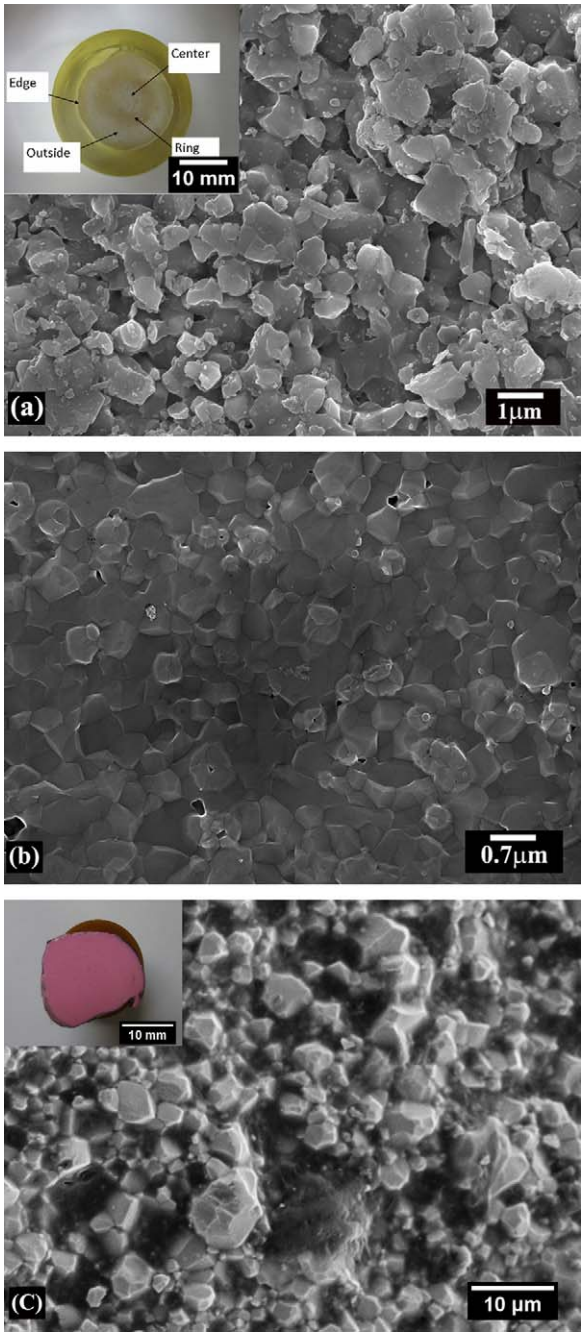

Fig. 2. Typical SEM micrographs of polycrystalline samples used herein of, (a) Center region in Sc_2O_3. Inset shows mounted sample with four tones of beige designated: Edge, Outside, Ring and Center; (b) Edge region in Sc_2O_3; (c) Er_2O_3. Inset shows pink polished sample glued to the NI sample holder.

The same parameters were used for the two diamond spherical tips (with radii of 1.4 μm and 5 μm), viz. 0.10 s^{-1} strain rate, 2 nm harmonic displacement target, and a frequency of 45 Hz. The maximum load used with the 5 μm tip was 80 mN; for the 1.4 μm tip it was 30 mN. In both cases the unloading rate was 2 mN/s. Four to ten different locations were typically indented to determine the elastic properties and the spherical NI stress/strain curves. For each location we performed a series of four successive loading and unloading cycles, the results of which were averaged.

In previous studies, we typically obtained the moduli of our surfaces – on mostly single crystals – from the slope of the S vs. a curves over their entire range. In the present study we first measured the dynamic modulus of our polycrystalline materials and then calculated E as done previously.[39] Briefly, E^*, was first obtained from the slopes of the S vs. a curves after which E was calculated from Eq. (4). For the 1.4 μm and 5 μm tips, we used the range of a up to $a \cong 800$ nm and $a \cong 1700$ nm, respectively. Above these limits, the indenters can no longer assumed to be spherical and Eq. (3) is no longer valid.[39] In all cases, the S vs. a data were zero-corrected.[33]

The point at which the NI stress–strain curves deviated from linearity,[27] was taken as the NI yield point, σ_y. The procedure followed here is the one proposed by Bushby[27] who studied metals. According to him the yield stress is determined at the point where the deviation from linearity occurs (Point B in his Fig. 10). The deviation was related to plasticity under the indenter. As noted above, we also examined the effect of surface roughness on the measured elastic moduli, yield and maximum stresses for each tip.

3.2.3. Berkovich and Vickers microhardness and indentation fracture toughness

A microhardness tester (M-400 Microhardness Tester, LECO, St. Joseph, MI) was used to measure the Vickers microhardness. Using a load of 3 N and a 15 s dwell time, the hardness values of six indents in each of the four Sc_2O_3 regions (inset in Fig. 2a) – for a total of 24 indents – were averaged. A total of six indents on Er_2O_3 were made using the same parameters. The Vickers microhardness, H_V, values were calculated using standard methods.[42]

The indentation fracture toughness, K_{IC} was evaluated from the hardness indents and the size of the crack extending from the corners of the indent according to the equations listed in Table 3.[43–49] Determination of twice the crack size, $2c$, was somewhat problematic, since as in some cases the cracks were not fully developed after unloading. To obtain the true crack lengths, the surface was polished for 60 s[39] using diamond paste (1 μm) and coolant liquid (Hyprez OS) which is oil based. One should be cautious not to remove material and alter the crack size, and not to use water or any other liquids that promote slow crack growth.

A Berkovich tip, whose total included angle and half-angles were, respectively, 142.3° and 65.35°, was used to calculate the Berkovich hardness, H_{Br}, and Berkovich Young's moduli, E_{Br}. These values were determined in the 100 nm $\leq h_t \leq$ 1500 nm range. This range was chosen because when the modulus vs. displacement curves were plotted (not shown), the E_{Br} values were nearly constant. The data collected from the NI was analyzed using the TestWorks™ software and the properties were calculated by well-established procedures.[26,29,31]

3.2.4. Optical microscopy and scanning electron microscopy

Both an optical microscope, OM (Olympus PMG3, Japan) and a scanning electron microscope, SEM (Zeiss Supra 50VP,

Table 3
Summary of equations used for the calculation of K_{IC} of Sc_2O_3 and Er_2O_3, where, P is the load applied in the Vickers hardness test (3 N), ϕ is a constraint factor ($\phi \sim 3$), E, is the Young's modulus, H, the Vickers hardness, c, the radius of the critical crack and, d, is half of the diagonal of the Vickers indent. The third and the fourth columns are the values for Sc_2O_3, the fifth and the sixth columns are for Er_2O_3.

Method	Mathematical expression		$Sc_2O_3 K_{IC}$ (MPa m$^{1/2}$)	$Er_2O_3 K_{IC}$ (MPa m$^{1/2}$)
Evans and Charles[44]	$K_{IC} = 0.16Hd^2C^{-3/2}$	(6)	1.12 ± 0.15	1.54 ± 0.12
Laugier[49]	$K_{IC} = 0.010\left(\frac{E}{H}\right)^{2/3}\left(\frac{P^{3/2}}{c}\right)$	(7)	1.14 ± 0.11	1.65 ± 0.12
Anstis et al.[46]	$K_{IC} = 0.016\left(\frac{E}{H}\right)^{0.5}\left(\frac{P^{1.5}}{c}\right)$	(8)	1.23 ± 0.12	1.77 ± 0.12
Niihara et al.[47]	$K_{IC} = \frac{0.129}{\phi}\left(\frac{c}{d}\right)^{-3/2} Hd^{1/2}\left(\frac{E\phi}{H}\right)^{0.4}$	(9)	1.57 ± 0.21	2.24 ± 0.18
Langford[48]	$K_{IC} = \frac{0.142}{\phi Hd^{3/2}}\left(\frac{E\phi}{H}\right)^{0.4}\left(\frac{c}{d}\right)^{-1.56}$	(10)	1.62 ± 0.23	2.36 ± 0.19

Thornwood, NY) were used to image the polished surfaces before, and after, the various indentations.

To measure the grain size, fractured surfaces were first etched by immersing them in boiling H_2SO_4 for 20 s. The average grain size was determined using the line-intercept method of SEM micrographs of etched fractured surfaces. For Sc_2O_3, multiple measurements were made on the four regions shown in inset in Fig. 2a. Three different micrographs were used for each region. In each micrograph, about 50 grains were measured. For Er_2O_3 about 40 grains were measured.

4. Results

4.1. Dynamic elastic moduli

The Sc_2O_3 sample's measured density, ρ, was $3833 \pm 1.4\,kg\,m^{-3}$. Since the theoretical density, ρ_T, calculated from the appropriate ICDD X-ray card is $3840\,kg\,m^{-3}$,[50] the relative density is >0.998. Based on the values of V_L and V_T – $8803 \pm 9\,ms^{-1}$ and $4801 \pm 4\,ms^{-1}$, respectively – and the sample's density, E^S and ν^S, were calculated according to the theory of elasticity[52] to be 227.6 ± 1 GPa and 0.288 ± 0.005, respectively.

The Er_2O_3 sample's density was $8530 \pm 9\,kg\,m^{-3}$. Given that the theoretical density of Er_2O_3, calculated from the appropriate ICDD X-ray card, is $8660\,kg\,m^{-3}$,[50] the relative density is >0.985. Based on the values of V_L and V_T – $5138 \pm 9\,ms^{-1}$ and $2750 \pm 3\,ms^{-1}$, respectively – and the sample's density, E^S and ν^S, were calculated to be 168.1 ± 0.8 GPa and 0.299 ± 0.005, respectively.

4.2. Young's moduli obtained from S vs. a curves

For both Sc_2O_3 and Er_2O_3 samples, the S vs. a curves – for the 1.4 μm and 5 μm indenters (Fig. 3) confirm that the relationship between S vs. a is indeed quite linear. The reproducibility of the curves in the various locations is noteworthy. For both tips, the E_{Sp} values are listed in Table 4. Clearly, tip size affects the moduli values. Also listed in Table 5 are the E_{Br} values for both materials.

4.3. NI stress–strain curves

Typical NI load–displacement curves, for both indenters – for the outer region of the Sc_2O_3 sample – are shown in Fig. 4. The corresponding stress–strain curves obtained using the 1.4 μm and 5 μm tips, are shown in Fig. 4b and c, respectively. Similar results (not shown) hold for the other areas. The stress–strain curves are characterized by a linear elastic region, followed by a plastic regime with little strain hardening. At strains >0.2, work hardening is apparent (Fig. 4b).

Typical NI load–displacement curves, for both indenters for Er_2O_3, are shown as an inset in Fig. 4. The corresponding stress–strain curves, obtained using for the 1.4 μm and 5 μm tips, are shown in Fig. 5a and b, respectively. Here again, a linear regime is followed by a plastic regime, with little strain hardening until a strain of ≈0.2.

The yield stresses, for both tips in the various locations are summarized in Table 5. The average grain sizes of the four

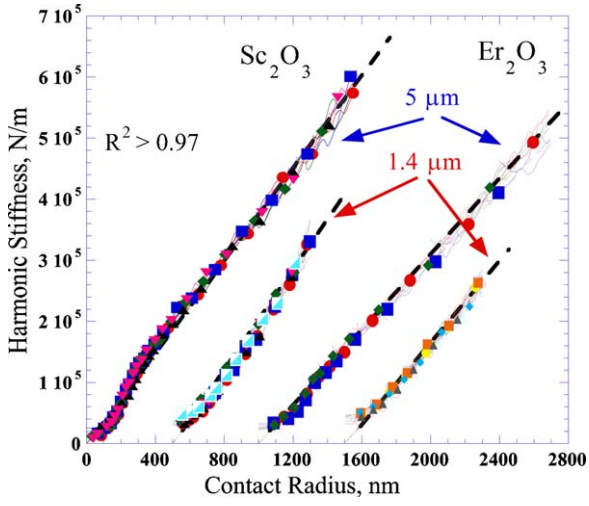

Fig. 3. Typical S vs. a plots in multiple locations obtained with the 1.4 μm and 5 μm tips for Sc_2O_3 and Er_2O_3. The data for the 5 μm tip in Sc_2O_3 and the 1.4 μm and 5 μm tips in Er_2O_3 are shifted to the right, respectively, by 500 nm, 1000 nm and 1500 nm for clarity. The slopes of the lines forced through zero – that equal $2E^*$ – are shown. In all cases, only 5% of data points collected are plotted for clarity's sake.

Table 4
Summary of the E values, in GPa, of Sc_2O_3 and Er_2O_3 calculated from the slopes of the S vs. a curves, the Berkovich method and the dynamic method. In all cases, the S vs. a slopes were zero corrected and forced through the origin.[39] The maximum loads used for these measurements were 30 mN and 80 mN for 1.4 μm and 5 μm tips, respectively. The Poisson's ratios assumed for Sc_2O_3 and Er_2O_3 were 0.288 and 0.299, respectively.

Location	Tip size		
	1.4 μm	5 μm	Berkovich
Sc_2O_3			
Edge	215 ± 4	205 ± 4	207 ± 2
Outside	218 ± 8	208 ± 3	210 ± 3
Ring	217 ± 6	209 ± 6	228 ± 3
Center	216 ± 6	211 ± 3	214 ± 5
Average[a]	*217 ± 6*	*210 ± 4*	*216 ± 8*
Dynamic		228 ± 1	
Er_2O_3			
Average	*164 ± 3*	*161 ± 5*	*172 ± 4*
Dynamic		168 ± 1	

Italic indicate that this is an average of average grain size ~0.75.
[a] This average is for the three major regions Outside, Ring and Center where the grain sizes are similar ~0.75 μm and the Edge is excluded, see Table 5.

regions of the Sc_2O_3 sample, listed in Table 5, range from a low of 0.48 ± 0.06 μm, to a high of 0.83 ± 0.07 μm. The average of the three major regions Outside, Ring and Center where the grain sizes are similar is 0.75 ± 0.07 μm. For Er_2O_3, the average grain size was 2.8 ± 0.4 μm (Fig. 2c).

4.4. Hardness and fracture toughness

Both the H_V and the H_{Br} values are listed in Table 5. The average H_{Br} values for both Sc_2O_3 and Er_2O_3 were 12.1 ± 0.5 GPa and 9.3 ± 1 GPa, respectively. At 10.8 ± 0.6 GPa and 7.5 ± 0.3 GPa, the average H_V values for Sc_2O_3 and Er_2O_3, respectively, are slightly lower. Short horizontal lines, labeled H_V and H_{Br}, appear near the y-axis in Figs. 4b and 5a.

The K_{IC} values for Sc_2O_3 and Er_2O_3 calculated – using Eqs. (6)–(10) listed in Table 3. The average K_{IC} values were calculated using E^S and their values were 1.35 ± 0.3 MPa $m^{1/2}$ and 1.9 ± 0.4 MPa $m^{1/2}$, respectively.

4.5. SEM

Typical SEM micrographs of a 5 μm indent loaded to 80 mN in Sc_2O_3 in shown in Fig. 6a. Inset shows a 1.4 μm indentation made in the same surface loaded to 30 mN. The corresponding SEM micrographs for Er_2O_3 are shown in Fig. 6b.

5. Discussion

5.1. Elastic moduli

At 227.6 ± 1 GPa, the E^S values obtained herein for Sc_2O_3 are in excellent agreement with the extrapolated value of 227 GPa for a pore free Sc_2O_3.[11] However, this value differs from the average evaluated value of 260 ± 37 GPa, reported in Section 1. This evaluated values is based on the equation $E = 3B(1 - 2\nu)$[51] and on the value of $\nu = 0.256$ reported by Dole et al.[11] The current ν for Sc_2O_3 measured here, 0.288, is slightly higher than the extrapolated value of 0.256 reported by Dole et al.[11] for fully dense Sc_2O_3.

Hence, if the measured ν, viz. 0.288, is used in the estimation, the average E decrease to 226 ± 32 GPa, which is consistent with the measured value in the present study. This fact is an indirect indication that the ν measured here, is probably more accurate than the one reported by Dole et al.,[11] but this requires further examination.

A perusal of Table 4 shows that E_{Sp} values calculated from S vs. a curves depend on tip size. For the Sc_2O_3, E_{Sp} underestimates E^S by ≈4%, and by ≈7%, respectively, for the 1.4 μm and 5 μm indenters. E_{Br} underestimate E^S by ≈6%. The best value obtained from the S vs. a curves, viz. 217 ± 6 GPa, is in excellent agreement with Gogotsi's value of 218 GPa,[3,22] and no worse or better than the E_{Br} value of 215 ± 9 GPa.

In the case of Er_2O_3, E_{Sp} obtained, viz. 164 ± 3 GPa (Table 4), is marginally smaller than the 168 ± 1 GPa obtained from ultrasound. The E_{Br} values, which range from 172 GPa and 177 GPa, are slightly higher. These moduli values are higher than those reported by Manning et al.[18] for 95% dense Er_2O_3, but lower than their extrapolated value for pore-free Er_2O_3 viz.

Table 5
Summary of NI yield stresses, σ_y [GPa], for Sc_2O_3 and Er_2O_3 as a function of spherical tip diameter and surface polishing conditions. Also listed in the last two columns are the Vickers [GPa] and Berkovich hardness [GPa] values measured on the same samples in the different locations designated. The last column lists the grain sizes of the various regions in Sc_2O_3 and the average grain size for Er_2O_3.

Location	Yield points, σ_y		Vickers hardness	Berkovich hardness	Grain size (μm)
	1.4 μm	5 μm			
Sc_2O_3					
Edge	8.2 ± 1.2	9.4 ± 0.5	11.5 ± 0.3	12.3 ± 0.3	0.48 ± 0.06
Outside	6.9 ± 0.6	8.4 ± 0.6	11.1 ± 0.6	12.1 ± 0.2	0.83 ± 0.07
Ring	7.0 ± 1.0	8.6 ± 0.8	10.4 ± 0.2	12.3 ± 0.3	0.69 ± 0.05
Center	7.3 ± 0.8	9.9 ± 0.7	10.3 ± 0.5	11.6 ± 0.5	0.73 ± 0.12
Average[a]	*7.0 ± 1.8*	*9.0 ± 0.9*	*10.6 ± 0.6*	*12.0 ± 0.5*	*0.75 ± 0.07*
Er_2O_3					
Average	*5.9 ± 0.7*	*6.5 ± 0.4*	7.5 ± 0.3	9.3 ± 1.0	*2.8 ± 0.4*

Italic indicate that this is an average of average grain size ~0.75.
[a] This average is for the three major regions Outside, Ring and Center where the grain sizes are similar ~0.75 μm and the Edge is excluded.

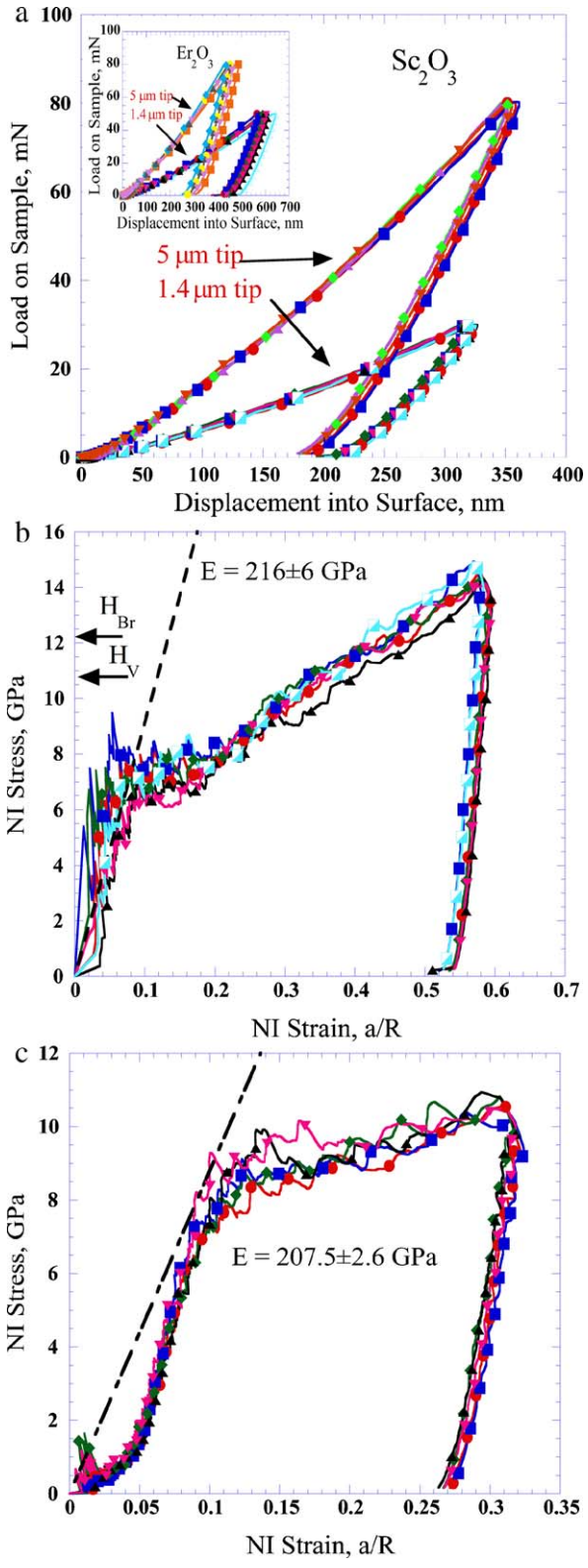

Fig. 4. (a) Load–displacement curves of the 1.4 μm and 5 μm tips indented into the Sc_2O_3 surface. Inset shows same results for Er_2O_3. (b) Typical NI stress–strain curves obtained when 1.4 μm spherical tip is indented into surface, (c) same as b, but using the 5 μm tip indenter. In all cases, only 5% of data points collected are plotted. Dashed inclined lines going through the origin represent the expected "ideal" stress–strain trajectory assuming the Young's modulus listed in the graph, viz. those listed in Table 5. H_{Br} and H_V denote the Berkovich and Vickers hardness values, respectively.

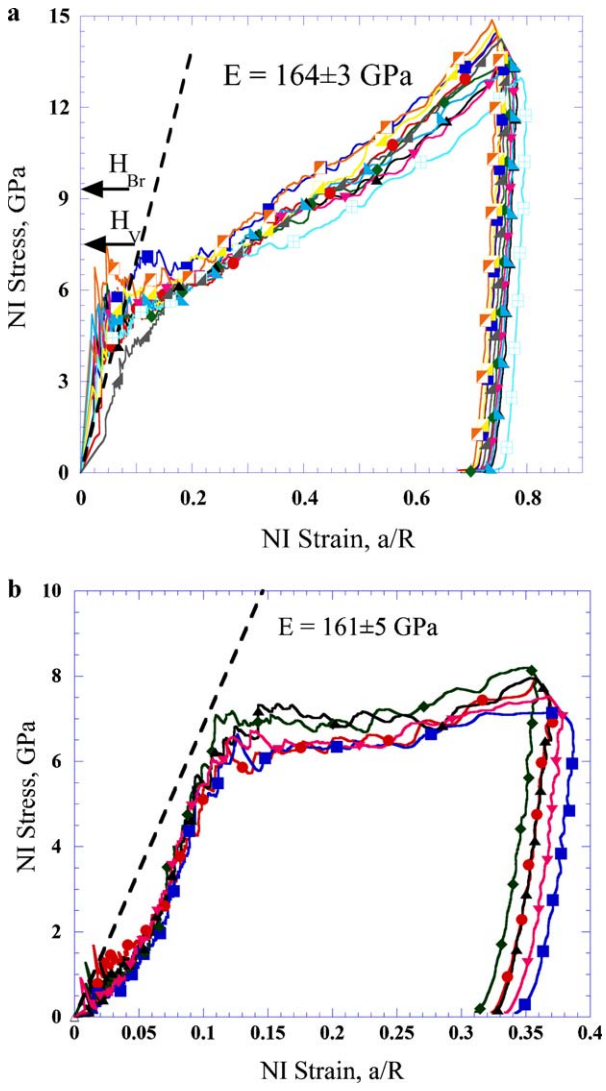

Fig. 5. Typical NI stress–strain curves in multiple locations obtained when Er_2O_3 sample is indented with, (a) 1.4 μm spherical tip, (b) 5 μm tip. In all cases, only 5% of data points collected are plotted. Dashed inclined lines going through the origin represent the expected "ideal" stress–strain trajectory assuming the Young's modulus shown in the graph, viz. those listed in Table 4. H_{Br} and H_V denote the Berkovich and Vickers hardness values, respectively.

175.2 GPa[18] or the 177.4 GPa value of Sharif et al.[14] The ν reported herein, viz. 0.299, is in between the values of 0.292 and 0.339 reported by Manning et al.[18] and Sharif et al.,[14] respectively. It follows that our values are thus quite reasonable.

5.2. NI stress–strain curves

From the results listed in Table 5 it is obvious that: (i) σ_y values at the edge of the Sc_2O_3 sample are higher than those in the center; (ii) σ_y values for the 1.4 μm tip are less than those for the 5 μm tip; (iii) An inverse correlation exists between σ_y and the grain sizes of the various location in the Sc_2O_3 sample; (iv) Like H_V and H_{Br} the σ_y's for Sc_2O_3 are higher than those for Er_2O_3; (v) From σ_y to a strain of about 0.2, the work hardening rate is quite low (e.g. Figs. 4c and 5b). At a strain of ≈0.2, the work hardening rate increases, more or less linearly, with

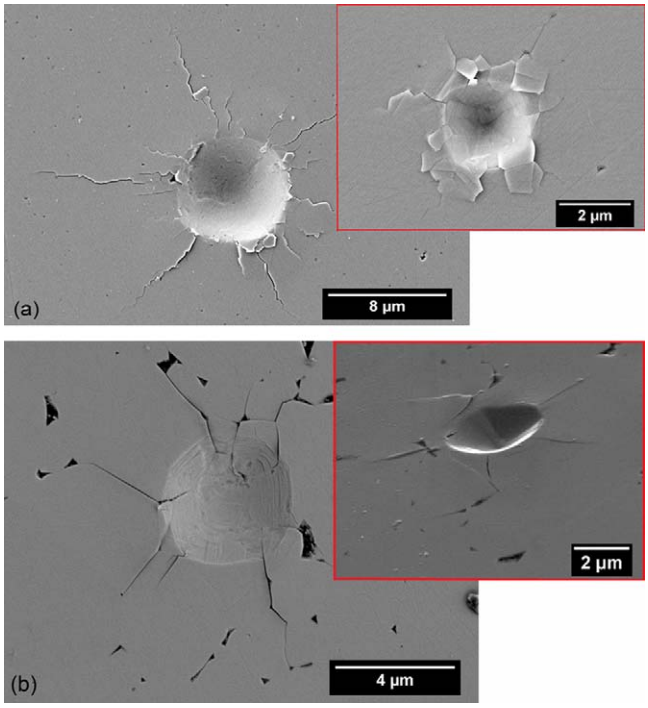

Fig. 6. Typical SEM micrographs of indentation marks made with, (a) 5 μm tip loaded to 80 mN in Sc_2O_3. Inset shows 1.4 μm indent in same surface loaded to 30 mN and, (b) 5 μm tip loaded to 80 mN in Er_2O_3. Inset shows 1.4 μm indent loaded to 50 mN.

stress (Figs. 4b and 5a); (vi) The order, from lower to higher is, $\sigma_y < H_V < H_{Br}$.

The inverse correlation between grain size and σ_y is intriguing and suggests a Hall-Petch like dependence.[52] To test this hypothesis, we plotted σ_y vs. the reciprocal of the square root of the grain size (Fig. 7). The decent correlation coefficient, $R^2 \sim 0.92$, suggests such a relationship may be valid. However, given that the range of grain sizes explored is quite narrow, the validity of this relationship needs to be explored over much wider grain sizes, using a larger variety of spherical indenter tip radii.

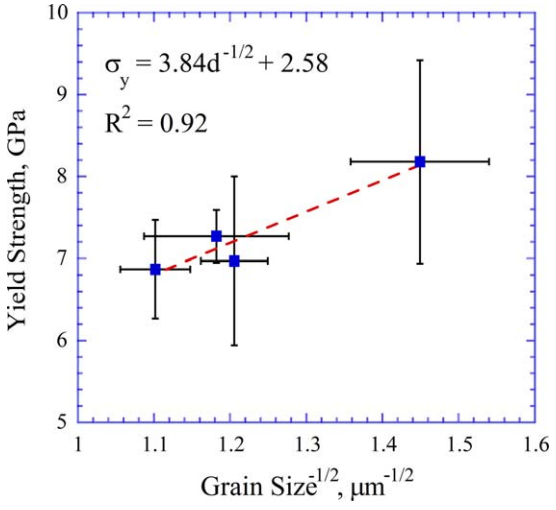

Fig. 7. Dependence of σ_y on reciprocal of square root of grain size in the various regions of the polished Sc_2O_3 surface.

Not surprisingly, H_V and H_{Br} are much less sensitive to grain size (Table 5).

This relationship, however, may explain another intriguing finding of this work, namely, the fact that σ_y's for the 5 μm tip indenter tip were higher than those of the 1.4 μm tip – an inverse tip size effect. Given the average grain sizes of the Sc_2O_3 and Er_2O_3 samples, it is reasonable to assume that the 1.4 μm indenter was exploring more the single crystal σ_y's than the 5 μm tip. Said otherwise, the probability of the 1.4 μm indenter hitting a single grain was higher than that of the 5 μm indenter. This is indirectly confirmed in the SEM micrographs (insets in Fig. 6a and b) where the indentation marks for the 1.4 μm tips are indeed of the same size of the grains; those of the 5 μm tip straddle a number of grains.

From σ_y to a strain of about 0.2, the work hardening rate is quite low (e.g. Figs. 4b and 5a). Since at relatively low deformation strains, it is reasonable to assume that the slip systems are non-intersecting. At a strain of ≈0.2, the work hardening rate increases, more or less linearly, with stress (Figs. 4b and 5b). As the plastic deformation is calculated out of the Herzian regime, herein we report the apparent strain hardening values. Least squares fits of the slopes of the stress–strain plots – from a strain of 0.2–0.5 for the fine polish and the 1.4 μm tip – for Sc_2O_3 and Er_2O_3 are 17.5 ± 1.3 GPa/strain and 12.5 ± 1.5 GPa/strain, respectively. These comments notwithstanding it is hereby acknowledged that these conjectures are preliminary and need to be more carefully studied and documented and extended to other grain sizes and indenter tip sizes before hard conclusions can be reached.

As noted above, and similar to most of our work to date,[32,39] the order of hardness values was, $\sigma_y < H_V < H_{Br}$. The reason for this state of affairs remains unclear. There are few possible reasons for this difference; the first one is because H_{Br} is measured at max load and H_V after deforming. The second one is that in the Vickers method, the projected area is used, while for the Berkovich, it is the actual contact area, A_C. However, if one uses the actual area for Vickers, viz. $A_C = A_P(\cos 68°)^{-1}$, the ratio, $A_C/A_P = 1.018$, is still significantly smaller than the ratio H_{Br}/H_V ∼1.13 and ∼1.24 attained for Sc_2O_3 and Er_2O_3, respectively (Table 5). The third suggested explanation is that, and for some unknown reason the strains that develop beneath a Berkovich indents are higher than those under a Vickers indents. This conclusion is best seen in Figs. 4b and 5a, where it is clear that the H_{Br} intersects the NI stress–strain curves at a strain of ≈0.45, while H_V intersects the latter at ≈0.3. The last possible explanation, is the fact that reports exist of excessive dislocation density under the Berkovich tip as compared the dislocation density under the Vickers tip.[53] In the latter article the authors calculate the strain created by the Vickers indenter $\varepsilon_V = 0.079$ and by the Berkovich indenter $\varepsilon_B = 0.103$ were obtained.[53] These comments notwithstanding, more work is needed to understand this fairly universal observation.

For Er_2O_3, the value of H_V measured herein, 7.5 ± 0.3 GPa, is consistent with value of 7 GPa reported for Er_2O_3 single crystals.[8,9] Similarly, H_V for Sc_2O_3 – 10.8 ± 0.6 GPa – is consistent with the values of 8.3 GPa and 11.4 GPa reported by Xu et al.[19] for thin films. The present result is also higher

than the value of 8.9 GPa reported by Gazza et al.[2] for hot pressed Sc_2O_3 with the slightly larger grain size of 1–2 μm. This difference might be consistent with the grain size differences.

5.3. Fracture toughness and hardness values

Using a value of E^S of 227.6 GPa, the fracture toughness of Sc_2O_3, obtained herein, viz. 1.35 ± 0.3 MPa $m^{1/2}$, are consistent with Gogotsi's[12] value of 1.49 ± 0.03 MPa $m^{1/2}$ for 98.7% dense Sc_2O_3 measured using single edge notched beam samples. The similarity of these results confirms the values of K_{IC} obtained herein from Vickers indentation.

Assuming a modulus of 168 GPa, the value of K_{IC} calculated for Er_2O_3 (Table 3) is 1.9 ± 0.4 MPa m; a value that is consistent with the results listed in Table 2 for high-density Er_2O_3.

6. Summary and conclusions

The Young's moduli, E, and nanoindentation stress–strain curves of fine-grained Sc_2O_3 and Er_2O_3 with grain sizes in the order of ~1–3 μm, were determined using a NI capable of continually measuring S. Two hemi-spherical indenters with radii, R, of 1.4 μm and 5 μm were used in addition to a Berkovich tip. We also measured the dynamic moduli of the same samples by ultrasound.

The elastic moduli measured with the 1.4 μm tip, were 217 ± 6 GPa and 164 ± 3 GPa for Sc_2O_3 and Er_2O_3, respectively. These values agreed well with those measured by a Berkovich tip, viz. 215 ± 6 GPa and 172 ± 4 GPa, respectively. These values were, in turn, in good agreement with the values measured by ultrasound, viz. 228 ± 1 GPa and 168 ± 1 GPa for Sc_2O_3 and Er_2O_3, respectively.

When the NI load–displacement curves were converted to NI stress–strain curves, the yield points were found to also be a function of tip radius. For the 5 μm tip, the yield points were 9.2 ± 0.7 GPa for Sc_2O_3 and 6.5 ± 0.5 GPa for Er_2O_3. The corresponding values for the 1.4 μm were roughly 20% lower. The Vickers hardness values of Sc_2O_3 and Er_2O_3 were 10.8 ± 0.6 GPa and 7.5 ± 0.3 GPa, respectively; the corresponding Berkovich values were 12.1 ± 0.6 GPa and 9.3 ± 1 GPa.

The fracture toughness values extracted from the Vickers indentations of Sc_2O_3 and Er_2O_3, were, respectively, 1.35 ± 0.3 MPa $m^{1/2}$ and 1.9 ± 0.4 MPa $m^{1/2}$-values that are comparable to the literature results for such polycrystalline samples.

Acknowledgements

This work was funded by the Army Research Office (W911NF-07-1-0628).

References

1. Cao X. Applications of rare earth in thermal barrier coating materials. *Journal of Materials Science and Technology* 2007;**23**(1):15–33.
2. Gazza GE, Roderick D, Levine B. Transparent Sc_2O_3 by hot-pressing. *Journal of Materials Science* 1971;**6**:1137–9.
3. Gogotsi GA. Thermal stress behaviour of yttria, scandia and AlN ceramics. *Ceramics International* 1980;**6**:31–5.
4. Barzilai S, Nagar H, Aizenshtein M, Froumin N, Frage N. Interface interaction and wetting of Sc_2O_3 exposed to Cu–Al and Cu–Ti melts. *Applied Physics A: Materials Science & Processing* 2009;**95**(2):507–12.
5. Lu J, Bisson JF, Takaichi K, Uematsu T, Shirakawa A, Musha M, Ueda K. Yb3+:Sc_2O_3 ceramic laser. *Applied Physics Letters* 2003;**83**:1101, doi:10.1063/1.1600851.
6. Tokurakowa M, Shirakawa A, Ueda K, Yagi H, Yanagitani T, Kaminskii AA. Diode-pumped sub-100 fs Kerr-lens mode-locked Yb3+:Sc_2O_3 ceramic laser. *Optics Letters* 2007;**32**:3382–4.
7. Li Ji-G, Ikegami T, Mori T. Fabrication of transparent, sintered Sc_2O_3 ceramics. *Journal of the American Ceramic Society* 2005;**88**(4):817–21.
8. Petrovic JJ, Romero RM, Mendoza D, Kukla AM, Hoover RC, McClellan KJ. Synthesis and properties of erbium oxide single crystal, Los Alamos LA-UR 99-479. *Ceramic Engineering Science Proceedings* 1999;**20**:3–10.
9. Petrovic JJ, Sharif AA, Kukla AM, Romero RM, Mendoza D, Pitek FM. *Mechanical behavior of erbium oxide single crystal*; 2000. Los Alamos LA-UR 00-318.
10. Gogotsi GA, private communication; 2008.
11. Dole SL, Hunter Jr O, Calderwood FW. Elastic properties of polycrystalline scandium and thulium oxides. *Journal of the American Ceramic Society – Discussion and Notes* 1977;**63**(3–4):167–8.
12. Gogotsi G, Mudrik S, Galenko V. Evaluation of fracture resistance of ceramics: edge fracture tests. *Ceramics International* 2007;**33**:315–20.
13. Elastic Moduli Data for Polycrystalline Ceramics, http://www.ceramics.nist.gov/srd/summary/emodox00.htm.
14. Sharif AA, Chu A, Misra F, Mitchell TE, Petrovic JJ. Elastic constants of erbia single crystals. *Journal of the American Ceramic Society* 2000;**83**(9):2246–50.
15. Makino Y, Miake S. Estimation of bulk moduli of compounds by empirical relations between bulk modulus and interatomic distance. *Journal of Alloys and Compounds* 2000;**313**:141–234.
16. Yusa H, Tsuchiya T, Sata N, Ohishi Y. High pressure transition to the Gd_2S_3 structure in Sc_2O_3: a new trend in dense structure I sesquioxide. *Inorganic Chemistry* 2009;**48**(16):7537–43.
17. Barzilai S, Halevy I, Yeheskel O, Bulk modulus of Sc_2O_3: *ab-initio* calculations and experimental results, unpublished results.
18. Manning WR, Hunter JR O, Powell JR BR. Elastic properties of polycrystalline yttrium oxide, dysprosium oxide, holmium oxide, and erbium oxide: room temperature measurements. *Journal of the American Ceramic Society* 1969;**52**(8):436–44.
19. Xu Z, Daga A, Chen H. Microstructure and optical properties of scandium oxide thin films prepared by metalorganic chemical-vapor deposition. *Applied Physics Letters* 2001;**79**(23):3782–90.
20. Neuman AD, Platero BM, Romero RS, McClellan KJ, Petrovic JJ. Mechanical properties of melt-derived erbium oxide. In: *22nd Annual Cocoa Beach Conference and Exposition*. 1998.
21. Neuman A, Platero M, Romero R, McClellan KJ, Petrovic JJ. Fabrication and properties of erbium oxide. In: *Proceedings of the 21st annual conference on composites, advanced ceramics, materials, and structures – B: ceramic engineering and science proceedings, vol. 18(4)*. 1997. p. 37–44.
22. Gogotsi G. Fracture resistance of ceramics: direct measurements. *Advances in Science and Technology* 2006;**45**:95–100.
23. Tabor D. *The hardness of metals*. Oxford: Clarendon Press; 1951. Oxford Classics Series 2000.
24. Field JS, Swain MV. Determining the mechanical properties of small volumes of material from sub-micrometer spherical indentations. *Journal of Materials Research* 1995;**10**:101.
25. Oliver WC, Pharr GM. An improved technique for determining hardness and elastic-modulus using load and displacement sensing indentation experiments. *Journal of Materials Research* 1992;**7**:1564–83.
26. Lawn BR. Indentation of ceramics with spheres: a century after Hertz. *Journal of the American Ceramic Society* 1998;**81**(8):1977–94.

27. Bushby AJ. Nano-indentation using spherical indenters. *Nondestructive Testing and Evaluation* 2001;**17**:213–34.
28. Li X, Bhushan B. A review of nanoindentation continuous stiffness measurement technique and its applications. *Materials Characterization* 2002;**48**:11–36.
29. Oliver WC, Pharr GM. Measurement of hardness and elastic modulus by instrumented indentation: advances in understanding and refinements to methodology. *Journal of Materials Research* 2004;**19**:3.
30. Fischer-Cripps AC. Review critical review of analysis and interpretation of nanoindentation test data. *Surface & Coatings Technology* 2006;**200**:4153–65.
31. Fischer-Cripps AC. Review of analysis methods for sub-micron indentation testing. *Vacuum* 2000;**58**(4):569–85.
32. Basu S, Moseson A, Barsoum MW. On the determination of spherical nanoindentation stress–strain curves. *Journal of Materials Research* 2006;**21**(10):2628–37.
33. Moseson AJ, Basu S, Barsoum MW. Determination of the effective zero point of contact for spherical nanoindentation. *Journal of Materials Research* 2008;**23**(1):204–9.
34. Basu S, Barsoum MW, Kalidindi SR. Sapphire: a kinking nonlinear elastic solid. *Journal of Applied Physics* 2006;**99**:063501.
35. Basu S, Barsoum MW. On the use of spherical nanoindentations to determine the deformation micromechanics of ZnO single crystals. *Journal of Materials Research* 2007;**22**:2470–7.
36. Buchs R, Basu S, Elshrief O, Coward R, Barsoum MW. Vickers and spherical nanoindentation study of the deformation of poled $BaTiO_3$ single crystals. *Journal of Applied Physics* 2009;**105**:093540.
37. Basu S, Zhou A, Barsoum MW. Reversible dislocation motion under contact loading in $LiNbO_3$ single crystals. *Journal of Materials Research* 2008;**23**:1134–8.
38. Basu S, Zhou A, Barsoum MW. On spherical nanoindentations, kinking nonlinear elasticity of mica single crystals and their geological implications. *Journal of Structural Geology* 2009;**31**:791–801.
39. Albayrak IC, Basu S, Sakulich A, Yeheskel O, Barsoum MW. Elastic and mechanical properties of polycrystalline transparent yttria as determined by indentation techniques. *Journal of the American Ceramic Society* 2010;**93**(7):2028–34.
40. Yeheskel O, Tevet O. Elastic moduli of transparent yttria. *Journal of the American Ceramic Society* 1999;**82**(1):136–44.
41. Yeheskel O, Shokhat M, Salhov S, Tevet O. Effect of initial particle and agglomerate size on the elastic moduli of porous yttria (Y_2O_3). *Journal of the American Ceramic Society* 2009;**92**(8):1655–62.
42. Quinn GD, Salem J, Bar-on I, Chu K, Foley M, Fang H. Fracture toughness of advanced ceramics at room temperature. *Journal of Research of the National Institute of Standards and Technology* 1992;**97**: 579–607.
43. Quinn GD, Bradt RC. On the Vickers indentation fracture toughness test. *Journal of the American Ceramic Society* 2007;**90**(3):673–80.
44. Evans AG, Charles EA. Fracture toughness determination by indentation. *Journal of the American Ceramic Society* 1976;**59**:371–2.
45. Lawn B, Evans AG, Marshall DB. Elastic/plastic indentation damage in ceramics: the median/radial crack system. *Journal of the American Ceramic Society* 1980;**63**:574.
46. Anstis GR, Chantikul P, Lawn BR, Marshall DB. *Journal of the American Ceramic Society* 1981;**64**:533.
47. Niihara K, Morena R, Hasselman DPH. Evaluation of K_{IC} of brittle solids by the indentation method with a low crack-to-indent ratios. *Journal of Material Science Letter* 1982;**1**:13–6.
48. Langford J. Indentation microstructure in Palmqvist crack regime: implications for fracture toughness evaluation by the indentation method. *Journal of Material Science Letter* 1982;**1**:493–5.
49. Laugier MT. The elastic/plastic indentation of ceramics. *Journal of Material Science Letter* 1985;**4**:1539–41.
50. The International Centre for Diffraction Data, ICDD, Sc_2O_3, card # 43-1028, Er_2O_3, card # 43-1007.
51. Timoshenko SP, Goodier JN. *Theory of elasticity*. New York: McGraw-Hill book Co.; 1972.
52. Guy AG. *Essentials of materials science international student edition*. Ltd Tokyo: McGraw-Hill Kogakusha; 1976.
53. Shikimaka O, Grabco D. Deformation created by Berkovich and Vickers indenters and its influence on surface morphology of indentations for LiF and CaF_2 single crystals. *Journal of Physics D: Applied Physics* 2008;**41**:074012 (6 pp.).